Improved measurements of branching fractions for $\eta_c \to \phi\phi$ and $\omega\phi$

M. Ablikim[1], M. N. Achasov[9,e], X. C. Ai[1], O. Albayrak[5], M. Albrecht[4], D. J. Ambrose[44], A. Amoroso[49A,49C], F. F. An[1], Q. An[46,a], J. Z. Bai[1], R. Baldini Ferroli[20A], Y. Ban[31], D. W. Bennett[19], J. V. Bennett[5], M. Bertani[20A], D. Bettoni[21A], J. M. Bian[43], F. Bianchi[49A,49C], E. Boger[23,c], I. Boyko[23], R. A. Briere[5], H. Cai[51], X. Cai[1,a], O. Cakir[40A], A. Calcaterra[20A], G. F. Cao[1], S. A. Cetin[40B], J. F. Chang[1,a], G. Chelkov[23,c,d], G. Chen[1], H. S. Chen[1], H. Y. Chen[2], J. C. Chen[1], M. L. Chen[1,a], S. Chen[41], S. J. Chen[29], X. Chen[1,a], X. R. Chen[26], Y. B. Chen[1,a], H. P. Cheng[17], X. K. Chu[31], G. Cibinetto[21A], H. L. Dai[1,a], J. P. Dai[34], A. Dbeyssi[14], D. Dedovich[23], Z. Y. Deng[1], A. Denig[22], I. Denysenko[23], M. Destefanis[49A,49C], F. De Mori[49A,49C], Y. Ding[27], C. Dong[30], J. Dong[1,a], L. Y. Dong[1], M. Y. Dong[1,a], Z. L. Dou[29], S. X. Du[53], P. F. Duan[1], J. Z. Fan[39], J. Fang[1,a], S. S. Fang[1], X. Fang[46,a], Y. Fang[1], R. Farinelli[21A,21B], L. Fava[49B,49C], O. Fedorov[23], F. Feldbauer[22], G. Felici[20A], C. Q. Feng[46,a], E. Fioravanti[21A], M. Fritsch[14,22], C. D. Fu[1], Q. Gao[1], X. L. Gao[46,a], X. Y. Gao[2], Y. Gao[39], Z. Gao[46,a], I. Garzia[21A], K. Goetzen[10], L. Gong[30], W. X. Gong[1,a], W. Gradl[22], M. Greco[49A,49C], M. H. Gu[1,a], Y. T. Gu[12], Y. H. Guan[1], A. Q. Guo[1], L. B. Guo[28], R. P. Guo[1], Y. Guo[1], Y. P. Guo[22], Z. Haddadi[25], A. Hafner[22], S. Han[51], X. Q. Hao[15], F. A. Harris[42], K. L. He[1], T. Held[4], Y. K. Heng[1,a], Z. L. Hou[1], C. Hu[28], H. M. Hu[1], J. F. Hu[49A,49C], T. Hu[1,a], Y. Hu[1], G. S. Huang[46,a], J. S. Huang[15], X. T. Huang[33], X. Z. Huang[29], Y. Huang[29], Z. L. Huang[27], T. Hussain[48], Q. Ji[1], Q. P. Ji[30], X. B. Ji[1], X. L. Ji[1,a], L. W. Jiang[51], X. S. Jiang[1,a], X. Y. Jiang[30], J. B. Jiao[33], Z. Jiao[17], D. P. Jin[1,a], S. Jin[1], T. Johansson[50], A. Julin[43], N. Kalantar-Nayestanaki[25], X. L. Kang[1], X. S. Kang[30], M. Kavatsyuk[25], B. C. Ke[5], P. Kiese[22], R. Kliemt[14], B. Kloss[22], O. B. Kolcu[40B,h], B. Kopf[4], M. Kornicer[42], A. Kupsc[50], W. Kühn[24], J. S. Lange[24], M. Lara[19], P. Larin[14], C. Leng[49C], C. Li[50], Cheng Li[46,a], D. M. Li[53], F. Li[1,a], F. Y. Li[31], G. Li[1], H. B. Li[1], H. J. Li[1], J. C. Li[1], Jin Li[32], K. Li[33], K. Li[13], Lei Li[3], P. R. Li[41], Q. Y. Li[33], T. Li[33], W. D. Li[1], W. G. Li[1], X. L. Li[33], X. N. Li[1,a], X. Q. Li[30], Y. B. Li[2], Z. B. Li[38], H. Liang[46,a], Y. F. Liang[36], Y. T. Liang[24], G. R. Liao[11], D. X. Lin[14], B. Liu[34], B. J. Liu[1], C. X. Liu[1], D. Liu[46,a], F. H. Liu[35], Fang Liu[1], Feng Liu[6], H. B. Liu[12], H. H. Liu[16], H. H. Liu[1], H. M. Liu[1], J. Liu[1], J. B. Liu[46,a], J. P. Liu[51], J. Y. Liu[1], K. Liu[39], K. Y. Liu[27], L. D. Liu[31], P. L. Liu[1,a], Q. Liu[41], S. B. Liu[46,a], X. Liu[26], Y. B. Liu[30], Z. A. Liu[1,a], Zhiqing Liu[22], H. Loehner[25], X. C. Lou[1,a,g], H. J. Lu[17], J. G. Lu[1,a], Y. Lu[1], Y. P. Lu[1,a], C. L. Luo[28], M. X. Luo[52], T. Luo[42], X. L. Luo[1,a], X. R. Lyu[41], F. C. Ma[27], H. L. Ma[1], L. L. Ma[33], M. M. Ma[1], Q. M. Ma[1], T. Ma[1], X. N. Ma[30], X. Y. Ma[1,a], Y. M. Ma[33], F. E. Maas[14], M. Maggiora[49A,49C], Y. J. Mao[31], Z. P. Mao[1], S. Marcello[49A,49C], J. G. Messchendorp[25], J. Min[1,a], T. J. Min[1], R. E. Mitchell[19], X. H. Mo[1,a], Y. J. Mo[6], C. Morales Morales[14], N. Yu. Muchnoi[9,e], H. Muramatsu[43], Y. Nefedov[23], F. Nerling[14], I. B. Nikolaev[9,e], Z. Ning[1,a], S. Nisar[8], S. L. Niu[1,a], X. Y. Niu[1], S. L. Olsen[32], Q. Ouyang[1,a], S. Pacetti[20B], Y. Pan[46,a], P. Patteri[20A], M. Pelizaeus[4], H. P. Peng[46,a], K. Peters[10,i], J. Pettersson[50], J. L. Ping[28], R. G. Ping[1], R. Poling[43], V. Prasad[1], H. R. Qi[2], M. Qi[29], S. Qian[1,a], C. F. Qiao[41], L. Q. Qin[33], N. Qin[51], X. S. Qin[1], Z. H. Qin[1,a], J. F. Qiu[1], K. H. Rashid[48], C. F. Redmer[22], M. Ripka[22], G. Rong[1], Ch. Rosner[14], X. D. Ruan[12], A. Sarantsev[23,f], M. Savrié[21B], K. Schoenning[50], S. Schumann[22], W. Shan[31], M. Shao[46,a], C. P. Shen[2], P. X. Shen[30], X. Y. Shen[1], H. Y. Sheng[1], M. Shi[1], W. M. Song[1], X. Y. Song[1], S. Sosio[49A,49C], S. Spataro[49A,49C], G. X. Sun[1], J. F. Sun[15], S. S. Sun[1], X. H. Sun[1], Y. J. Sun[46,a], Y. Z. Sun[1], Z. J. Sun[1,a], Z. T. Sun[19], C. J. Tang[36], X. Tang[1], I. Tapan[40C], E. H. Thorndike[44], M. Tiemens[25], M. Ullrich[24], I. Uman[40D], G. S. Varner[42], B. Wang[30], B. L. Wang[41], D. Wang[31], D. Y. Wang[31], K. Wang[1,a], L. L. Wang[1], L. S. Wang[1], M. Wang[33], P. Wang[1], P. L. Wang[1], W. Wang[1,a], W. P. Wang[46,a], X. F. Wang[39], Y. Wang[37], Y. D. Wang[14], Y. F. Wang[1,a], Y. Q. Wang[22], Z. Wang[1,a], Z. G. Wang[1,a], Z. H. Wang[46,a], Z. Y. Wang[1], Z. Y. Wang[1], T. Weber[22], D. H. Wei[11], P. Weidenkaff[22], S. P. Wen[1], U. Wiedner[4], M. Wolke[50], L. H. Wu[1], L. J. Wu[1], Z. Wu[1,a], L. Xia[46,a], L. G. Xia[39], Y. Xia[18], D. Xiao[1], H. Xiao[47], Z. J. Xiao[28], Y. G. Xie[1,a], Q. L. Xiu[1,a], G. F. Xu[1], J. J. Xu[1], L. Xu[1], Q. J. Xu[13], Q. N. Xu[41], X. P. Xu[37], L. Yan[49A,49C], W. B. Yan[46,a], W. C. Yan[46,a], Y. H. Yan[18], H. J. Yang[34,j], H. X. Yang[1], L. Yang[51], Y. X. Yang[11], M. Ye[1,a], M. H. Ye[7], J. H. Yin[1], B. X. Yu[1,a], C. X. Yu[30], J. S. Yu[26], C. Z. Yuan[1], W. L. Yuan[29], Y. Yuan[1], A. Yuncu[40B,b], A. A. Zafar[48], A. Zallo[20A], Y. Zeng[18], Z. Zeng[46,a], B. X. Zhang[1], B. Y. Zhang[1,a], C. Zhang[29], C. C. Zhang[1], D. H. Zhang[1], H. H. Zhang[38], H. Y. Zhang[1,a], J. Zhang[1], J. J. Zhang[1], J. L. Zhang[1], J. Q. Zhang[1], J. W. Zhang[1,a], J. Y. Zhang[1], J. Z. Zhang[1], K. Zhang[1], L. Zhang[1], S. Q. Zhang[30], X. Y. Zhang[33], Y. Zhang[1], Y. H. Zhang[1,a], Y. N. Zhang[41], Y. T. Zhang[46,a], Yu Zhang[41], Z. H. Zhang[6], Z. P. Zhang[46], Z. Y. Zhang[51], G. Zhao[1], J. W. Zhao[1,a], J. Y. Zhao[1], J. Z. Zhao[1,a], Lei Zhao[46,a], Ling Zhao[1], M. G. Zhao[30], Q. Zhao[1], Q. W. Zhao[1], S. J. Zhao[53], T. C. Zhao[1], Y. B. Zhao[1,a], Z. G. Zhao[46,a], A. Zhemchugov[23,c], B. Zheng[47], J. P. Zheng[1,a], W. J. Zheng[33], Y. H. Zheng[41], B. Zhong[28], L. Zhou[1,a], X. Zhou[51], X. K. Zhou[46,a], X. R. Zhou[46,a], X. Y. Zhou[1], K. Zhu[1], K. J. Zhu[1,a], S. Zhu[1], S. H. Zhu[45], X. L. Zhu[39], Y. C. Zhu[46,a], Y. S. Zhu[1], Z. A. Zhu[1], J. Zhuang[1,a], L. Zotti[49A,49C], B. S. Zou[1], J. H. Zou[1]

(BESIII Collaboration)

[1] *Institute of High Energy Physics, Beijing 100049, People's Republic of China*
[2] *Beihang University, Beijing 100191, People's Republic of China*
[3] *Beijing Institute of Petrochemical Technology, Beijing 102617, People's Republic of China*
[4] *Bochum Ruhr-University, D-44780 Bochum, Germany*
[5] *Carnegie Mellon University, Pittsburgh, Pennsylvania 15213, USA*
[6] *Central China Normal University, Wuhan 430079, People's Republic of China*
[7] *China Center of Advanced Science and Technology, Beijing 100190, People's Republic of China*
[8] *COMSATS Institute of Information Technology, Lahore, Defence Road, Off Raiwind Road, 54000 Lahore, Pakistan*
[9] *G.I. Budker Institute of Nuclear Physics SB RAS (BINP), Novosibirsk 630090, Russia*
[10] *GSI Helmholtzcentre for Heavy Ion Research GmbH, D-64291 Darmstadt, Germany*
[11] *Guangxi Normal University, Guilin 541004, People's Republic of China*
[12] *Guangxi University, Nanning 530004, People's Republic of China*
[13] *Hangzhou Normal University, Hangzhou 310036, People's Republic of China*
[14] *Helmholtz Institute Mainz, Johann-Joachim-Becher-Weg 45, D-55099 Mainz, Germany*
[15] *Henan Normal University, Xinxiang 453007, People's Republic of China*
[16] *Henan University of Science and Technology, Luoyang 471003, People's Republic of China*
[17] *Huangshan College, Huangshan 245000, People's Republic of China*
[18] *Hunan University, Changsha 410082, People's Republic of China*
[19] *Indiana University, Bloomington, Indiana 47405, USA*
[20] *(A)INFN Laboratori Nazionali di Frascati, I-00044 Frascati, Italy; (B)INFN and University of Perugia, I-06100 Perugia, Italy*
[21] *(A)INFN Sezione di Ferrara, I-44122 Ferrara, Italy; (B)University of Ferrara, I-44122 Ferrara, Italy*
[22] *Johannes Gutenberg University of Mainz, Johann-Joachim-Becher-Weg 45, D-55099 Mainz, Germany*
[23] *Joint Institute for Nuclear Research, 141980 Dubna, Moscow region, Russia*
[24] *Justus-Liebig-Universitaet Giessen, II. Physikalisches Institut, Heinrich-Buff-Ring 16, D-35392 Giessen, Germany*
[25] *KVI-CART, University of Groningen, NL-9747 AA Groningen, Netherlands*
[26] *Lanzhou University, Lanzhou 730000, People's Republic of China*
[27] *Liaoning University, Shenyang 110036, People's Republic of China*
[28] *Nanjing Normal University, Nanjing 210023, People's Republic of China*
[29] *Nanjing University, Nanjing 210093, People's Republic of China*
[30] *Nankai University, Tianjin 300071, People's Republic of China*
[31] *Peking University, Beijing 100871, People's Republic of China*
[32] *Seoul National University, Seoul 151-747, Korea*
[33] *Shandong University, Jinan 250100, People's Republic of China*
[34] *Shanghai Jiao Tong University, Shanghai 200240, People's Republic of China*
[35] *Shanxi University, Taiyuan 030006, People's Republic of China*
[36] *Sichuan University, Chengdu 610064, People's Republic of China*
[37] *Soochow University, Suzhou 215006, People's Republic of China*
[38] *Sun Yat-Sen University, Guangzhou 510275, People's Republic of China*
[39] *Tsinghua University, Beijing 100084, People's Republic of China*
[40] *(A)Ankara University, 06100 Tandogan, Ankara, Turkey; (B)Istanbul Bilgi University, 34060 Eyup, Istanbul, Turkey; (C)Uludag University, 16059 Bursa, Turkey; (D)Near East University, Nicosia, North Cyprus, Mersin 10, Turkey*
[41] *University of Chinese Academy of Sciences, Beijing 100049, People's Republic of China*
[42] *University of Hawaii, Honolulu, Hawaii 96822, USA*
[43] *University of Minnesota, Minneapolis, Minnesota 55455, USA*
[44] *University of Rochester, Rochester, New York 14627, USA*
[45] *University of Science and Technology Liaoning, Anshan 114051, People's Republic of China*
[46] *University of Science and Technology of China, Hefei 230026, People's Republic of China*
[47] *University of South China, Hengyang 421001, People's Republic of China*
[48] *University of the Punjab, Lahore 54590, Pakistan*
[49] *(A)University of Turin, I-10125, Turin, Italy; (B)University of Eastern*

Piedmont, I-15121, Alessandria, Italy; (C)INFN, I-10125 Turin, Italy
[50] *Uppsala University, Box 516, SE-75120 Uppsala, Sweden*
[51] *Wuhan University, Wuhan 430072, People's Republic of China*
[52] *Zhejiang University, Hangzhou 310027, People's Republic of China*
[53] *Zhengzhou University, Zhengzhou 450001, People's Republic of China*

[a] *Also at State Key Laboratory of Particle Detection and Electronics, Beijing 100049, Hefei 230026, People's Republic of China*
[b] *Also at Bogazici University, 34342 Istanbul, Turkey.*
[c] *Also at the Moscow Institute of Physics and Technology, Moscow 141700, Russia*
[d] *Also at the Functional Electronics Laboratory, Tomsk State University, Tomsk, 634050, Russia*
[e] *Also at the Novosibirsk State University, Novosibirsk 630090, Russia.*
[f] *Also at the NRC Kurchatov Institute, PNPI, 188300 Gatchina, Russia.*
[g] *Also at University of Texas at Dallas, Richardson, Texas 75083, USA.*
[h] *Also at Istanbul Arel University, 34295 Istanbul, Turkey.*
[i] *Also at Goethe University Frankfurt, 60323 Frankfurt am Main, Germany.*
[j] *Also at Institute of Nuclear and Particle Physics, Shanghai Key Laboratory for Particle Physics and Cosmology, Shanghai 200240, People's Republic of China.*

(Dated: May 2, 2017)

Using $(223.7 \pm 1.4) \times 10^6$ J/ψ events accumulated with the BESIII detector, we study η_c decays to $\phi\phi$ and $\omega\phi$ final states. The branching fraction of $\eta_c \to \phi\phi$ is measured to be $Br(\eta_c \to \phi\phi) = (2.5 \pm 0.3^{+0.3}_{-0.7} \pm 0.6) \times 10^{-3}$, where the first uncertainty is statistical, the second is systematic, and the third is from the uncertainty of $Br(J/\psi \to \gamma\eta_c)$. No significant signal for the double Okubo-Zweig-Iizuka suppressed decay of $\eta_c \to \omega\phi$ is observed, and the upper limit on the branching fraction is determined to be $Br(\eta_c \to \omega\phi) < 2.5 \times 10^{-4}$ at the 90% confidence level.

PACS numbers: 13.25.Gv, 13.20.Gd

I. INTRODUCTION

Our knowledge of the η_c properties is still relatively poor, although it has been established for more than thirty years [1]. Until now, the exclusively measured decays only sum up to about 63% of its total decay width [2]. The branching fraction of $\eta_c \to \phi\phi$ was measured for the first time by the MarkIII collaboration [3], and improved measurements were performed at BESII [4, 5] with a precision of about 40%. The decay $\eta_c \to \omega\phi$, which is a doubly Okubo-Zweig-Iizuka (OZI) suppressed process, has not been observed yet.

Decays of η_c into vector meson pairs have stood as a bewildering puzzle in charmonium physics for a long time. This kind of decay is highly suppressed at leading order in Quantum Chromodynamics (QCD), due to the helicity selection rule (HSR) [6]. Under HSR, the branching fraction for $\eta_c \to \phi\phi$ was calculated to be $\sim 2 \times 10^{-7}$ [7]. To avoid the manifestation of HSR in charmonium decays, a HSR evasion scenario was proposed [8]. Improved calculations with next-to-leading order [9] and relativistic corrections in QCD yield branching fractions varying from 10^{-5} [10] to 10^{-4} [11]. Some nonperturbative mechanisms, such as the light quark mass corrections [12], the $^3P_0$ quark pair creation mechanism [13] and long-distance intermediate meson loop effects [14], have also been phenomenologically investigated.

However, the measured branching fraction, $Br(\eta_c \to \phi\phi) = (1.76 \pm 0.20) \times 10^{-3}$ [2, 15], is much larger than those of theoretical predictions. To help understand the η_c decay mechanism, high precision measurements of the branching fraction are desirable. In this paper, we present an improved measurement of the branching fraction of $\eta_c \to \phi\phi$, and a search for the doubly OZI suppressed decay $\eta_c \to \omega\phi$. The analyses are performed based on $(223.7 \pm 1.4) \times 10^6$ J/ψ events [16] collected with the BESIII detector.

II. DETECTOR AND MONTE CARLO SIMULATION

The BESIII experiment at BEPCII [17] is an upgrade of BESII/BEPC [18]. The detector is designed to study physics in the τ-charm energy region [19]. The cylindrical BESIII detector is composed of a helium gas-based main drift chamber (MDC), a time-of-flight (TOF) system, a CsI (Tl) electromagnetic calorimeter (EMC) and a resistive-plate-chamber-based muon identifier with a superconducting magnet that provides a 1.0 T magnetic field. The nominal geometrical acceptance of the detector is 93% of 4π solid angle. The MDC measures the momentum of charged particles with a resolution of 0.5% at 1 GeV/c, and provides energy loss (dE/dx) measurements with a resolution better than 6% for electrons from Bhabha scattering. The EMC detects photons with a resolution of 2.5% (5%) at an energy of 1 GeV in the barrel (end cap) region.

To optimize event selection criteria and to understand backgrounds, a GEANT4-based [20] Monte Carlo (MC) simulation package, BOOST, which includes the description of the geometries and material as well as the BESIII detection components, is used to generate MC samples. An inclusive J/ψ-decay MC sample is generated to study the potential backgrounds. The production of the J/ψ resonance is simulated with the MC event generator KKMC [21], while J/ψ decays are simulated with BESEVTGEN [22] for known decay modes by setting the branching fractions to the world average values [2], and with LUNDCHARM [23] for the remaining unknown decays. The analysis is performed in the framework of the BESIII offline software system [24], which handles the detector calibration, event reconstruction and data storage.

III. EVENT SELECTION

The η_c candidates studied in this analysis are produced by J/ψ radiative transitions. We search for $\eta_c \to \phi\phi$ and $\omega\phi$ from the decays $J/\psi \to \gamma\phi\phi$ and $\gamma\omega\phi$, with final states of $\gamma 2(K^+K^-)$ and $3\gamma K^+K^-\pi^+\pi^-$, respectively. The candidate events are required to have four charged tracks with a net charge of 0, and at least one or three photons, respectively.

Charged tracks in the polar angle region $|\cos\theta| < 0.93$ are reconstructed from the MDC hits. They must have the point of closest approach to the interaction point within ± 10 cm along the beam direction and 1 cm in the plane perpendicular to the beam direction. For the particle identification (PID), the ionization energy deposited (dE/dx) in the MDC and the TOF information are combined to determine confidence levels (C.L.) for the pion and kaon hypotheses, and each track is assigned to the particle type with the highest PID C.L. For the decay $J/\psi \to \gamma\omega\phi \to 3\gamma K^+K^-\pi^+\pi^-$, two identified kaons are required within the momentum range of 0.3−0.9 GeV with an average efficiency of about 8%. For the decay $J/\psi \to \gamma\phi\phi \to \gamma 2(K^+K^-)$, no PID is required. The intermediate states, ϕ and ω, are selected using invariant mass requirements.

Photon candidates are reconstructed by clustering energy deposits in the EMC crystals. The energy deposited in the nearby TOF counters is included to improve the photon reconstruction efficiency and energy resolution. The photon candidates are required to be in the barrel region ($|\cos\theta| < 0.8$) of the EMC with at least 25 MeV total energy deposition, or in the end cap regions ($0.86 < |\cos\theta| < 0.92$) with at least 50 MeV total energy deposition, where θ is the polar angle of the photon. The photon candidates are, furthermore, required to be separated from all charged tracks by an angle larger than 10° to suppress photons radiated from charged particles. The photons in the regions between the barrel and end caps are poorly measured and, therefore, excluded. Timing information from the EMC is used to suppress electronic noise and showers that are unrelated to the event.

Kinematic fits, constrained by the total e^+e^- beam energy momentum, are performed under the $J/\psi \to \gamma 2(K^+K^-)$ and $3\gamma K^+K^-\pi^+\pi^-$ hypotheses. Fits are done with all photon combinations together with the four charged tracks. Only the combination with the smallest kinematic fit χ^2_{4C} is retained for further analysis, and $\chi^2_{4C} < 100$ (40) for $J/\psi \to \gamma 2(K^+K^-)$ ($3\gamma K^+K^-\pi^+\pi^-$) is required. These requirements are determined from MC simulations by optimizing $S/\sqrt{S+B}$, where S and B are the numbers of signal and background events, respectively.

Two ϕ candidates in the $J/\psi \to \gamma\phi\phi$ decay are reconstructed from the selected $2(K^+K^-)$ tracks. Only the combination with a minimum of $|M^{(1)}_{K^+K^-} - M_\phi|^2 + |M^{(2)}_{K^+K^-} - M_\phi|^2$ is retained, where $M^{(i)}_{K^+K^-}$ $(i = 1, 2)$ and M_ϕ denote the invariant mass of the K^+K^- pair and the nominal mass of the ϕ-meson, respectively. A scatter plot of $M^{(1)}_{K^+K^-}$ versus $M^{(2)}_{K^+K^-}$ for the surviving events is shown in Fig. 1 (a). There is a cluster of events in the $\phi\phi$ region indicated as a box in Fig. 1 (a) originating from the decay $J/\psi \to \gamma\phi\phi$. Two ϕ candidates are selected by requiring $|M_{K^+K^-} - M_\phi| < 0.02$ GeV/c^2, which is determined by optimizing $S/\sqrt{S+B}$, also.

For the decay $J/\psi \to \gamma\omega\phi \to \gamma K^+K^-\pi^+\pi^-\pi^0$, the photon combination with mass closest to the π^0 nominal mass is chosen, and $|M_{\gamma\gamma} - M_{\pi^0}| < 0.02$ GeV/c^2 is required. A scatter plot of the $M_{K^+K^-}$ versus $M_{\pi^+\pi^-\pi^0}$ for the surviving events is shown in Fig. 1 (b). Three vertical bands, as indicated in the plot, correspond to the η, ω and ϕ decays into $\pi^+\pi^-\pi^0$, and the horizontal band corresponds to the decay $\phi \to K^+K^-$. For the selection of $J/\psi \to \gamma\omega\phi$ candidates, the ϕ and ω requirements are determined, by optimizing $S/\sqrt{S+B}$, to be $|M_{\pi^+\pi^-\pi^0} - M_\omega| < 0.03$ GeV/c^2 and $|M_{K^+K^-} - M_\phi| < 0.008$ GeV/c^2.

IV. DATA ANALYSIS

A. Observation of $\eta_c \to \phi\phi$

Figure 2 shows the invariant mass distribution of the $\phi\phi$-system within the range from 2.7 to 3.1 GeV/c^2. The η_c signal is clearly observed. Background events from J/ψ decays are studied using the inclusive MC sample. The dominant backgrounds are from the decays $J/\psi \to \gamma\phi K^+K^-$ and $J/\psi \to \gamma K^+K^-K^+K^-$ with or without an η_c intermediate state, which have exactly the same final state as the signal, and are the peaking and non peaking backgrounds in the $2(K^+K^-)$ invariant mass distribution. In addition, there are 43 background events from the decays $J/\psi \to \phi f_1(1420)/f_1(1285)$ with f_1 decay to $K^+K^-\pi^0$ and $J/\psi \to \phi K^*(892)^\pm K^\mp$ with $K^*(892)^\pm$ decay to $K^\pm\pi^0$, which have a final state of $\pi^0 2(K^+K^-)$ similar to that of the signal. These background decay channels have low detection efficiency ($< 0.1\%$), and do not produce a peak in the η_c signal range. The expected

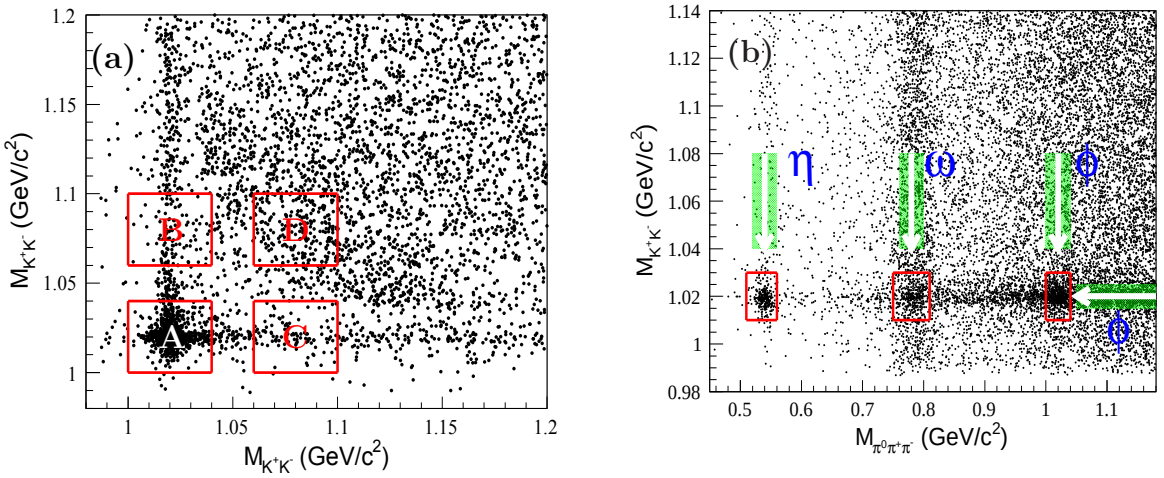

Fig. 1: Scatter plot of (a) $M^{(1)}_{K^+K^-}$ versus $M^{(2)}_{K^+K^-}$ for the decay $J/\psi \to \gamma 2(K^+K^-)$, and (b) $M_{K^+K^-}$ versus $M_{\pi^+\pi^-\pi^0}$ for the decay $J/\psi \to 3\gamma K^+K^-\pi^+\pi^-$.

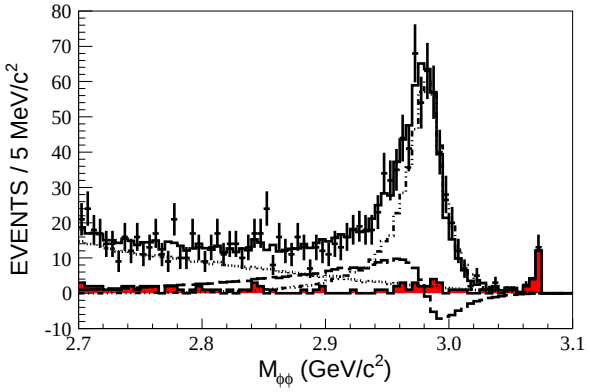

Fig. 2: Projection of fit results onto the $M_{\phi\phi}$ spectrum. The dots with error bars denote the data, the solid line histogram is the overall result, the dot-dashed histogram is the η_c signal, the filled red histogram is the combined backgrounds estimated with exclusive MC simulations, the dotted histogram denotes non η_c decays, and the long-dash histogram is the interference between the η_c and non η_c decays.

yields of background events are 26 and 75 for the peaking and non peaking backgrounds, respectively, determined with MC simulation. As a cross-check, the backgrounds are also estimated with the events in the ϕ sidebands region in data, and then using the MC information of the $\eta_c \to \phi K^+K^-$ and $2(K^+K^-)$ to scale the η_c events in boxes B, C and D to the signal region A, and total 104 events are obtained.

To determine the $\eta_c \to \phi\phi$ yield, an amplitude analysis is performed on the selected candidate 1,276 events. We assume the observed candidates are from the process $J/\psi \to \gamma\phi\phi$ with or without the η_c intermediate state in the $\phi\phi$ system. The amplitude formulas are constructed with the helicity-covariant method [25], and shown in the appendix. The η_c resonance is parametrized with the Breit-Wigner function multiplied by a damping factor

$$f(s) = \frac{1}{M^2 - s - iM\Gamma}\frac{\mathcal{F}(E_\gamma)}{\mathcal{F}(E^0_\gamma)}, \qquad (1)$$

where s is the square of $\phi\phi$ invariant mass, and M and Γ are the η_c mass and width, respectively. The damping factor is taken as $\mathcal{F}(E_\gamma) = \exp(-\frac{E^2_\gamma}{16\beta^2})$ with $\beta = 0.065$ GeV [26], and the photon energy E^0_γ corresponds to the $\sqrt{s} = M$.

In the analysis, the decay $J/\psi \to \gamma\eta_c \to \gamma\phi\phi$ and the nonresonant decays $J/\psi \to \gamma\phi\phi$ with different quantum numbers J^P (spin parity) in the $\phi\phi$ system are taken into consideration. The differential cross section $d\sigma/d\Omega$ is calculated with

$$\frac{d\sigma}{d\Omega} = \sum_{\text{helicities}} |A_{\eta_c}(\lambda_0,\lambda_\gamma,\lambda_1,\lambda_2) + \sum_{J^P} A^{J^P}_{NR}(\lambda_0,\lambda_\gamma,\lambda_1,\lambda_2)|^2, \qquad (2)$$

where A_{η_c} is the amplitude for the $J/\psi(\lambda_0) \to \gamma(\lambda_\gamma)\eta_c \to \gamma\phi(\lambda_1)\phi(\lambda_2)$, with the joint helicity angle Ω, and $A^{J^P}_{NR}$ is the amplitude for the nonresonant decay $J/\psi \to \gamma\phi\phi$ with J^P for the $\phi\phi$ system. To simplify the fit, only the nonresonant components with $J^P = 0^+$, 0^- and 2^+ are included, and the components with higher spin are ignored. The symmetry of the identical particles for the $\phi\phi$-meson pair is implemented in the amplitude.

The magnitudes and phases of the coupling constants are determined with an unbinned maximum likelihood fit to the selected candidates. The likelihood function

for observing the N events in the data sample is

$$\mathcal{L} = \prod_{i=1}^{N} P(x_i), \tag{3}$$

where $P(x_i)$ is the probability to observe event i with four momenta $x_i = (p_\gamma, p_\phi, p_\phi)_i$, which is the normalized differential cross section taking into account the detection efficiency (ϵ_i), and calculated by

$$P(x_i) = \frac{(d\sigma/d\Omega)_i \epsilon_i}{\sigma_{MC}}, \tag{4}$$

where the normalization factor σ_{MC} can be calculated by a signal MC sample $J/\psi \to \gamma\phi\phi$ with N_{MC} accepted events. These events are generated with a phase space model and then subjected to the detector simulation, and passed through the same events selection criteria as applied to the data. With a MC sample which is sufficiently large, σ_{MC} is evaluated with

$$\sigma_{MC} = \frac{1}{N_{MC}} \sum_{i=1}^{N_{MC}} \left(\frac{d\sigma}{d\Omega}\right)_i. \tag{5}$$

For a given N events data sample, the product of ϵ_i in Eq.(3) is constant, and can be neglected in the fit. Rather than maximizing $\mathcal{L}$, $\mathcal{T} = -\ln\mathcal{L}$ is minimized using MINUIT [27].

In the analysis, the background contribution to the log-likelihood value ($\ln\mathcal{L}_{\rm bkg}$) is subtracted from the log-likelihood value of data ($\ln\mathcal{L}_{\rm data}$), i.e. $\ln\mathcal{L} = \ln\mathcal{L}_{\rm data} - \ln\mathcal{L}_{\rm bkg}$, where $\ln\mathcal{L}_{\rm bkg}$ is estimated with the MC simulated background events, normalized to 101 events including peaking and nonpeaking η_c background.

In the fit, the mass and width of η_c are fixed to the previous BESIII measurements [28], i.e. $M = 2.984$ GeV/c^2 and $\Gamma = 0.032$ GeV. The mass resolution of the η_c is not considered in the nominal fit, and its effect is considered as a systematic uncertainty. The fit results are shown in Fig. 2, where the rightmost peak is due to backgrounds from $J/\psi \to \phi K^+K^-$ decay. The η_c yield from the fit is $N_{\eta_c} = 549 \pm 65$, which is derived from numerical integration of the resultant amplitudes, and the statistical error is derived from the covariance matrix obtained from the fit.

To determine the goodness of fit, a global $\chi^2_{\rm g}$ is calculated by comparing data and fit projection histograms, defined as

$$\chi^2_{\rm g} = \sum_{j=1}^{5} \chi^2_j, \text{ with } \chi^2_j = \sum_{i=1}^{N} \frac{(N^{\rm DT}_{ji} - N^{\rm Fit}_{ji})^2}{N^{DT}_{ji}}, \tag{6}$$

where $N^{\rm DT}_{ji}$ and $N^{\rm Fit}_{ji}$ are the numbers of events in the ith bin of the jth kinematic variable distribution. If $N^{\rm DT}_{ji}$ is sufficiently large, the $\chi^2_{\rm g}$ is expected to statistically follow the χ^2 distribution function with the number of degrees of freedom (ndf), which is the total number of bins in histograms minus the number of free parameters in the fit. In a histogram, bins with less than ten events are merged with the nearby bins. The individual χ^2_j give a qualitative evaluation of the fit quality for each kinematic variable, as described in the following.

Five independent variables are necessary to describe the three-body decay $J/\psi \to \gamma\phi\phi$. These are chosen to be the mass of the $\phi\phi$-system ($M_{\phi\phi}$), the mass of the $\gamma\phi$-system ($M_{\gamma\phi}$), the polar angle of the γ (θ_γ), the polar angle (θ_ϕ) and azimuthal angle (φ_ϕ) of the ϕ-meson, where the angles are defined in the J/ψ rest frame. Figure 3 shows the comparison of the distributions of $M_{\gamma\phi}$ and angles between the global fit and the data. A sum of all of the χ^2_j values gives $\chi^2_{\rm g} = 215$ with ndf=191. The quality of the global fit ($\chi^2_{\rm g}$/ndf) is 1.1, which indicates good agreement between data and the fit results.

To validate the robustness of the fit procedure, a pseudodata sample is generated with the amplitude model with all parameters fixed to the fit results. A total of 2936 events are selected with the same selection criteria as applied to the data. An identical fit process is carried out, and the ratio of output η_c signal yield to input number of events is 1.03 ± 0.03.

B. Search for $\eta_c \to \omega\phi$

Figure 4 shows the $\omega\phi$ invariant mass distribution in the range from 2.70 to 3.05 GeV/c^2 for the selected candidate events of $J/\psi \to \gamma\omega\phi$, and no significant η_c signal is observed. The background events from J/ψ decays are dominated by $J/\psi \to \eta'\phi$ with $\eta' \to \gamma\omega$. A small amount of background is from the decays $J/\psi \to f_0(980)\omega \to K^+K^-\omega$ and $J/\psi \to f_X\omega \to \pi^0K^+K^-\omega$, where f_X stands for the $f_1(1285)$ and $f_1(1420)$ resonances. The sum of all above backgrounds estimated from inclusive MC samples is small compared to the total number of selected candidates and appears as a flat $M_{\omega\phi}$ distribution, as shown in Fig. 4.

To set an upper limit for the branching fraction $Br(\eta_c \to \omega\phi)$, the signal yield is calculated at the 90% C.L. by a Bayesian method [2], according to the distribution of normalized likelihood values versus signal yield, which is obtained from the fits by fixing the η_c signal yield at different values.

In the fit, the shape for the η_c signal is described by the MC simulated line shape by setting the mass and width of η_c to the BESIII measurement [28]; the known background estimated with MC simulation is fixed in shape and magnitude in the fit; and the others are described by a second-order Chebychev function with floating parameters. The distribution of normalized likelihood values is shown in Fig. 5, and the upper limit of signal yield at the 90% C.L. is calculated to be 18.

To check the robustness of the event selection criteria, especially the dependence on $Br(\eta_c \to \omega\phi)$, the requirements of kinematic fit χ^2 and ϕ/ω mass windows are reoptimized with the measured upper limit. The η_c

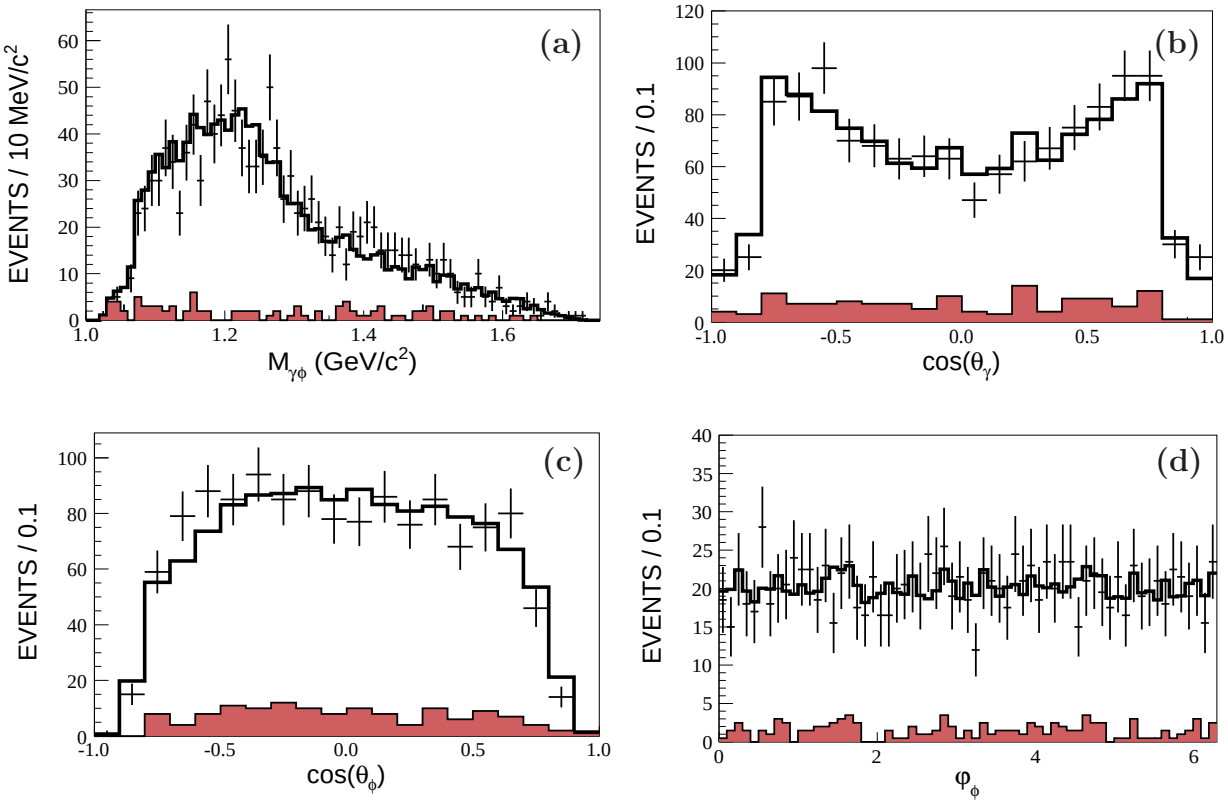

Fig. 3: Distributions of (a) the $\gamma\phi$ invariant mass $M_{\gamma\phi}$; (b) the polar angular of the photon $\cos\theta_\gamma$; (c) the polar angular of ϕ mesons $\cos\theta_\phi$; (d)and the azimuthal angular of ϕ mesons φ_ϕ. The dots with error bar are the data, the solid line histograms represent the total fit results, and the filled histograms are the non-$J/\psi \to \gamma\phi\phi$ backgrounds estimated with the exclusive MC samples.

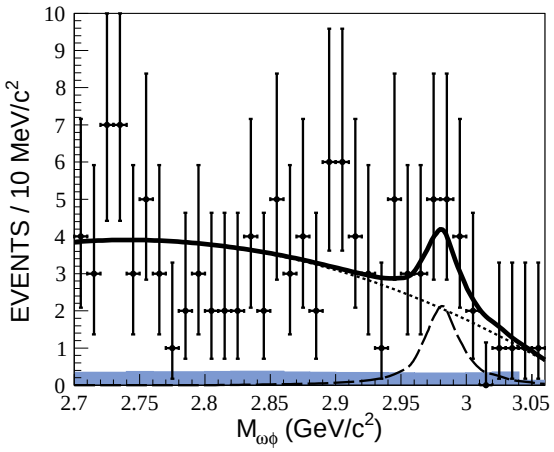

Fig. 4: Results of the best fit to the $M_{\omega\phi}$ distribution. Dots with error bars are data, the solid curve is the best fit result, corresponding to a η_c signal yield of 10 ± 6 events, the shaded histogram is the background estimated from exclusive MC samples, the dashed curve indicates the η_c signal, and the dotted curve is the fitted background.

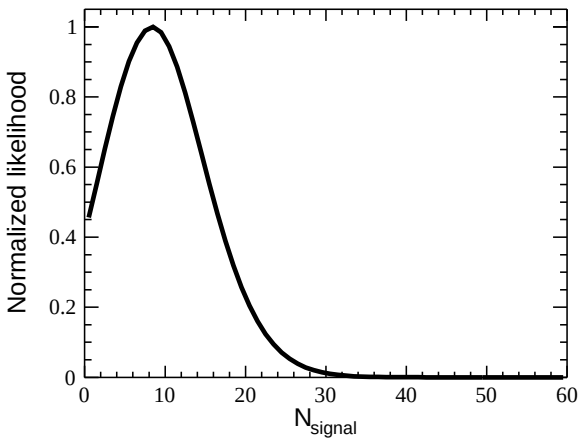

Fig. 5: Normalized likelihood distribution versus the η_c yield for $\eta_c \to \omega\phi$.

signal yield is reestimated and is consistent within the statistical errors.

V. SYSTEMATIC UNCERTAINTIES

The following sources of systematic uncertainties are considered in the measurements of branching fractions.

1. Number of J/ψ events

The number of J/ψ events is determined using its hadronic decays. The uncertainty is 0.6% [16].

2. Photon detection efficiency
The soft and hard photon detection efficiencies are studied using the control samples $\psi' \to \pi^0\pi^0 J/\psi$, with J/ψ decay e^+e^- or $\mu^+\mu^-$ and $J/\psi \to \rho\pi \to \pi^+\pi^-\pi^0$, respectively. The difference in the photon detection efficiency between the MC simulation and data is 1%, which is taken as the systematic uncertainty.

3. Kaon/pion tracking and PID efficiency
The uncertainties of kaon/pion tracking and PID efficiency are studied using the control samples $J/\psi \to \pi^+\pi^- p\bar{p}$ and $J/\psi \to K^0_S K\pi$, with the decay $K^0_S \to \pi^-\pi^+$ [29]. The uncertainties for tracking and PID efficiencies are both determined to be 1% per track.

4. Branching fractions
The uncertainties of branching fractions for $J/\psi \to \gamma\eta_c$, $\phi \to K^+K^-$, and $\omega \to \pi^+\pi^-\pi^0$ are taken from the PDG [2].

5. Kinematic fit
To estimate the uncertainty associated with the χ^2 requirement of the kinematic fit for the final state $\gamma 2(K^+K^-)$, we select the candidate events of $J/\psi \to \gamma\phi\phi$ by requiring $\chi^2 < 20$, 60 or 150, and the η_c signal yields are reestimated with amplitude analysis. The largest deviation to the nominal branching fraction, 6.7%, is taken as the systematic uncertainty.

For the final states $\gamma K^+K^-\pi^+\pi^-\pi^0$, we redetermine the upper limit on the branching fraction with the alternative requirement of the kinematic fit $\chi^2 < 20, 30, 50$ or 60, and the largest deviation to the nominal value, 2.4% at $\chi^2 < 30$, is taken as the systematic uncertainty.

6. Mass window
The uncertainties associated with the ϕ/ω mass-window requirement arise if the mass resolution is not consistent between the data and MC simulation. The uncertainty related to the ϕ-mass window requirement is determined with the control sample $\psi' \to \gamma\chi_{cJ}$, $\chi_{cJ} \to \phi\phi$, and $\phi \to K^+K^-$. The difference in ϕ-selection efficiency is estimated to be 0.7% and 1.1% for the $\eta_c \to \phi\phi$ and $\eta_c \to \omega\phi$ modes, respectively, where the different uncertainties obtained for the two decay modes are due to the different mass-window requirements. The uncertainty related with the ω mass-window requirement is determined with the control sample $J/\psi \to \omega\eta$ with $\omega \to \pi^+\pi^-\pi^0$ and $\eta \to \pi^+\pi^-\pi^0$. The difference in ω selection efficiency is estimated to be 1.5% for the $\eta_c \to \omega\phi$ mode.

7. Background
In the analysis of $J/\psi \to \gamma\phi\phi$, the uncertainty associated with the peaking background from $J/\psi \to \gamma\eta_c$, $\eta_c \to \phi K^+K^-$, and $2(K^+K^-)$ as well as the other unknown background is estimated by varying up or down the numbers of background events by one standard deviation according to the uncertainties of branching fractions in PDG [2]. The largest change in the $\eta_c \to \phi\phi$ signal yield is determined to be 0.9%, and is taken as the systematic uncertainty.

In the study of $J/\psi \to \gamma\omega\phi$, the uncertainty associated with the unknown background is estimated by replacing the second-order Chebychev function with the first-order one. The change of the upper limit of signal events is negligible. The uncertainty associated with the dominant background, $J/\psi \to \eta'\phi \to \gamma\omega\phi$, is estimated by varying the branching fraction by one standard deviation when normalizing the background in the fit. The difference in the resulting upper limit is determined to be 5.6%, and is taken as the systematic uncertainty.

8. Fit range
In the nominal fit, the fit range is set to be $M_{\phi\phi}$ and $M_{\omega\phi} > 2.70$ GeV/c^2. Its uncertainty is estimated by setting the range of $M_{\phi\phi}$ and $M_{\omega\phi} >$ 2.60, 2.65, 2.75 or 2.80 GeV/c^2. The branching fraction of $\eta_c \to \phi\phi$ and the upper limit for $\eta_c \to \omega\phi$ are reestimated. The largest deviations to the nominal results, 0.7% for the decay $\eta_c \to \phi\phi$ and 0.2% for the decay $\eta_c \to \omega\phi$, are taken as the systematic uncertainties.

9. η_c mass and width
Uncertainties associated with the η_c mass and width are estimated by the alternative fits with the PDG values for the η_c parameters [2]. The resulting differences in the η_c signal yield, 1.3% for $\eta_c \to \phi\phi$ and 5.6% for $\eta_c \to \omega\phi$, are taken as systematic uncertainties.

10. Amplitude analysis
Systematic uncertainties associated with the amplitude analysis arise including the uncertainties of the non-η_c component and the mass resolution of η_c.

In the nominal fit, the non-η_c component is described by the nonresonant $\phi\phi$-system assigned with quantum number $J^P = 0^-$, 0^+ and 2^+. The statistical significance for the component with different J^P is determined according to the difference of log-likelihood value between the cases with and without this component included in the fit, taking into account the change in the number of degrees of freedom. The significances for the non-η_c component with $J^P = 0^-$, 2^+, 0^+ are 2.8σ, 3.0σ and 0.1σ, respectively. If the 0^- component is removed, the uncertainty is estimated to be +6.7%. If the 2^+

TABLE I: Summary of all systematic uncertainties from the different resources (%). The combined uncertainty excludes the uncertainty associated with $Br(J/\psi \to \gamma\eta_c)$, which is given separately.

Sources	$\eta_c \to \phi\phi$	$\eta_c \to \omega\phi$
$N_{J/\psi}$	0.6	0.6
Photon	1.0	3.0
Tracking	4.0	4.0
PID	—	4.0
$Br(\phi \to K^+K^-)$	2.0	1.0
$Br(\omega \to \pi^+\pi^-\pi^0)$	—	0.8
Kinematic fit	6.7	2.4
$M_{K^+K^-}$ mass	0.7	1.1
$M_{\pi^+\pi^-\pi^0}$ mass	—	1.5
Background	0.9	5.6
Fit range	0.7	0.2
η_c mass and width	1.3	5.6
Amplitude analysis	$^{+7.1}_{-26.1}$	—
Combined	$^{+11.0}_{-27.4}$	10.7
$Br(J/\psi \to \gamma\eta_c)$	23.5	23.5

component is removed, the uncertainty is estimated to be -26.0% mainly due to the strong interference between the η_c and the 0^- components.

The uncertainty related with the η_c mass resolution is estimated by the alternative amplitude analysis with the detected width of the η_c set to 34.2 MeV, estimated from the MC simulation with the nominal input η_c width 32.0 MeV from Ref. [28]. The resulting difference of the η_c signal yield with respect to the nominal value is 2.2%.

The total uncertainty from the amplitude analysis is estimated to be $^{+7.1\%}_{-26.1\%}$.

Table I summarizes all sources of systematic uncertainties. The combined uncertainty is the quadratic sum of all uncertainties except for that associated with $Br(J/\psi \to \gamma\eta_c)$.

VI. BRANCHING FRACTIONS

A. $\eta_c \to \phi\phi$

The product branching fraction of $J/\psi \to \gamma\eta_c \to \gamma\phi\phi$ is calculated by

$$Br(J/\psi \to \gamma\eta_c)Br(\eta_c \to \phi\phi) = \frac{N_{\rm sig}}{N_{J/\psi}\epsilon Br^2(\phi \to K^+K^-)} = (4.3 \pm 0.5({\rm stat})^{+0.5}_{-1.2}({\rm syst})) \times 10^{-5},$$

where $Br(\phi \to K^+K^-)$ is the branching fraction of the $\phi \to K^+K^-$ decay taken from the PDG [2], $N_{\rm sig}$ is the η_c signal yield, and $\epsilon = 24\%$ is the detection efficiency, determined with the MC sample generated with the amplitude model with parameters fixed according to the fit results. The number of J/ψ events is $N_{J/\psi} = 223.7 \times 10^6$ [16].

Using $Br(J/\psi \to \gamma\eta_c) = (1.7 \pm 0.4)\%$ [2], $Br(\eta_c \to \phi\phi)$ is calculated to be

$$Br(\eta_c \to \phi\phi) = (2.5 \pm 0.3({\rm stat})^{+0.3}_{-0.7}({\rm syst}) \pm 0.6({\rm Br})) \times 10^{-3},$$

where the third uncertainty, which is dominant, is from the uncertainty of $Br(J/\psi \to \gamma\eta_c)$, and the second uncertainty is the quadratic sum of all other systematic uncertainties.

B. $\eta_c \to \omega\phi$

No significant signal is observed for $\eta_c \to \omega\phi$, and we determine the upper limit at the 90% C.L. for its branching fraction,

$$Br(\eta_c \to \omega\phi) < \frac{N_{\rm up}}{N_{J/\psi}\epsilon Br(1-\sigma_{\rm sys})} = 2.5 \times 10^{-4}, \quad (7)$$

where $N_{\rm up} = 18$ is the upper limit on the number of η_c events at the 90% C.L., $\epsilon = 5.9\%$ is the detection efficiency, $\sigma_{\rm sys} = 25.8\%$ is the total systematic error, and Br is the product branching fractions for the decay $J/\psi \to \gamma\eta_c$, $\phi \to K^+K^-$ and $\omega \to \pi^+\pi^-\pi^0$ [2].

VII. SUMMARY AND DISCUSSION

Using 223.7 million J/ψ events accumulated with the BESIII detector, we perform an improved measurement on the decay of $\eta_c \to \phi\phi$. The measured branching fraction is listed in Table II, and compared with the previous measurements. Within one standard deviation, our result is consistent with the previous measurements, but the precision is improved. No significant signal for $\eta_c \to \omega\phi$ is observed. The upper limit at the 90% C.L. on the branching fraction is determined to be $Br(\eta_c \to \omega\phi) < 2.5 \times 10^{-4}$, which is 1 order in magnitude more stringent than the previous upper limit [2].

The measured branching fractions of $\eta_c \to \phi\phi$ are three times larger than that calculated by next-to-leading perturbative QCD (pQCD) together with higher twist contributions [10]. This discrepancy between data and the HSR expectation [6] implies that nonperturbative mechanisms play an important role in charmonium decay. To understand the HSR violation mechanism, a comparison between the experimental measurements and the theoretical predictions based on the light quark mass correction [12], the $^3P_0$ quark pair creation mechanism [13] and the intermediate meson loop effects [14] is presented in Table II. We note that the measured $Br(\eta_c \to \phi\phi)$ is close to the predictions of the $^3P_0$ quark model [13] and the meson loop effects [14]. In addition, the measured upper limit for $Br(\eta_c \to \omega\phi)$ is comparable with the predicted value 3.25×10^{-4} in Ref. [14]. The consistency between

TABLE II: Comparison of BESIII measured $Br(\eta_c \to \phi\phi)$ with the previous results and theoretical predictions, where the branching fractions of $\eta_c \to \phi\phi$ from BESII and DM2 are recalculated with $\mathrm{Br}(J/\psi \to \gamma\eta_c) = (1.7 \pm 0.4)\%$ [2].

Experiment	$Br(J/\psi \to \gamma\eta_c)Br(\eta_c \to \phi\phi)(\times 10^{-5})$	$Br(\eta_c \to \phi\phi)$ $(\times 10^{-3})$
BESIII	$4.3 \pm 0.5^{+0.5}_{-1.2}$	$2.5 \pm 0.3^{+0.3}_{-0.7} \pm 0.6$
BESII [5]	3.3 ± 0.8	1.9 ± 0.6
DM2 [30]	3.9 ± 1.1	2.3 ± 0.8
Theoretical	Prediction	$Br(\eta_c \to \phi\phi)$ $(\times 10^{-3})$
	pQCD[10]	$(0.7 \sim 0.8)$
	$^3P_0$ quark model [13]	$(1.9 \sim 2.0)$
	Charm meson loop [14]	2.0

data and the theoretical calculation indicates the importance of QCD higher twist contributions or the presence of a non-pQCD mechanism.

VIII. ACKNOWLEDGMENT

The BESIII collaboration thanks the staff of BEPCII and the IHEP computing center for their strong support. This work is supported in part by National Key Basic Research Program of China under Contract No. 2015CB856700; National Natural Science Foundation of China (NSFC) under Contracts No. 11505034, No. 11375205, No. 11565006, No. 11647309, No. 11125525, No. 11235011, No. 11322544, No. 11335008, No. 11425524, and No. 11305090; the Chinese Academy of Sciences (CAS) Large-Scale Scientific Facility Program; the CAS Center for Excellence in Particle Physics (CCEPP); the Collaborative Innovation Center for Particles and Interactions (CICPI); Joint Large-Scale Scientific Facility Funds of the NSFC and CAS under Contracts No. 11179007, No. U1232201, and No. U1332201; CAS under Contracts No. KJCX2-YW-N29, and No. KJCX2-YW-N45; 100 Talents Program of CAS; National 1000 Talents Program of China; INPAC and Shanghai Key Laboratory for Particle Physics and Cosmology; German Research Foundation DFG under Collaborative Research Contract No. CRC 1044, and No. FOR 2359; Istituto Nazionale di Fisica Nucleare, Italy; Koninklijke Nederlandse Akademie van Wetenschappen (KNAW) under Contract No. 530-4CDP03; Ministry of Development of Turkey under Contract No. DPT2006K-120470; Russian Foundation for Basic Research under Contract No. 14-07-91152; the Swedish Resarch Council; U. S. Department of Energy under Contracts No. DE-FG02-05ER41374, No. DE-SC-0010504, No. de-sc0012069, and No. DESC0010118; U.S. National Science Foundation; University of Groningen (RuG) and the Helmholtzzentrum fuer Schwerionenforschung GmbH (GSI), Darmstadt; and WCU Program of National Research Foundation of Korea under Contract No. R32-2008-000-10155-0.

Appendix

Amplitude analysis of the decays $J/\psi \to \gamma\phi\phi$

A. AMPLITUDES

For the decay $J/\psi(\lambda_0) \to \gamma(\lambda_\gamma)\eta_c \to \gamma\phi(\lambda_1)\phi(\lambda_2)$, where the $\lambda_i (i = \gamma, 0, 1, 2)$ indicates helicity values for the corresponding particles, the helicity-coupling amplitude is given by

$$\begin{aligned} A_{\eta_c}(\lambda_0, \lambda_\gamma, \lambda_1, \lambda_2) &= F^{\psi}_{\lambda_\gamma}(r_1) D^{1*}_{\lambda_0, -\lambda_\gamma}(\theta_0, \phi_0) BW_j(m_{\phi\phi}) \\ &\times F^{\eta_c}_{\lambda_1, \lambda_2}(r_2) D^{0*}_{0, \lambda_1 - \lambda_2}(\theta_1, \phi_1) \frac{\mathcal{F}(E_\gamma)}{\mathcal{F}(E^0_\gamma)}, \end{aligned} \tag{8}$$

where $r_1(r_2)$ is the momentum difference between γ and η_c (two ϕ mesons) in the rest frame of J/ψ (η_c), and θ_0 (ϕ_0) and θ_1 (ϕ_1) are the polar (azimuthal) angles of the momentum vectors $\mathbf{P}_{\eta_c}$ and $\mathbf{P}_\phi$ in the helicity system of J/ψ and η_c, respectively. The z-axis defined for $\eta_c \to \phi(\lambda_1)\phi(\lambda_2)$ is taken along the outgoing direction of $\phi(\lambda_1)$ in the η_c rest frame, and the x-axis is in the $\mathbf{P}_{\eta_c}$ and $\mathbf{P}_{\phi(\lambda_1)}$ plane, which together with the new y-axis forms a right-hand system. $BW_j(m)$ denotes the Breit-Wigner parametrization for the η_c peak. The damping factor $\mathcal{F}(E_\gamma)$ is taken as $\mathcal{F}(E_\gamma) = \exp(-\frac{E^2_\gamma}{16\beta^2})$ with β=0.065 GeV [26]; E^0_γ is the photon energy corresponding to $m_{\phi\phi} = m_{\eta_c}$. The helicity-coupling amplitudes $F^{\psi}_{\lambda_\gamma}$ and $F^{\eta_c}_{\lambda_1,\lambda_2}$ are related to the covariant amplitudes in the LS-coupling scheme by [25]

$$\begin{aligned} F^{\psi}_{1} &= -F^{\psi}_{-1} = \frac{g_{11}}{\sqrt{2}} r_1 \frac{B_1(r_1)}{B_1(r^0_1)}, \\ F^{\eta_c}_{1,1} &= -F^{\eta_c}_{-1,-1} = \frac{g'_{11}}{\sqrt{2}} r_2 \frac{B_1(r_2)}{B_1(r^0_2)}, \\ F^{\eta_c}_{0,0} &= 0, \end{aligned} \tag{9}$$

where $B_l(r)$ is the Blatt-Weisskopf factor [25], r^0_1 and r^0_2 indicate the momentum differences for the two decays with $m_{\phi\phi} = m_{\eta_c}$, and g_{ls} and g'_{ls} are the coupling constants for the two decays.

For the direct decay $J/\psi \to \gamma\phi\phi$, the mass spectrum of $\phi\phi$ appears as a smooth distribution within the η_c signal region; hence the Breit-Wigner function is excluded. The amplitudes for the direct decay are decomposed into partial waves associated with the $\phi\phi$-system with quantum numbers $J^P = 0^-$, 0^+ and 2^+, and the high spin waves are neglected. These amplitudes are taken as

$$\begin{aligned}
A^{0^-}_{NR}(\lambda_0,\lambda_\gamma,\lambda_1,\lambda_2) &= F^{\psi}_{\lambda_\gamma,0} D^{1*}_{\lambda_0,-\lambda_\gamma}(\theta_0,\phi_0) F^{0^-}_{\lambda_1,\lambda_2} \\
&\times D^{0*}_{0,\lambda_1-\lambda_2}(\theta_1,\phi_1) \text{ for } 0^-, \\
A^{0^+}_{NR}(\lambda_0,\lambda_\gamma,\lambda_1,\lambda_2) &= F^{\psi}_{\lambda_\gamma,0} D^{1*}_{\lambda_0,-\lambda_\gamma}(\theta_0,\phi_0) F^{0^+}_{\lambda_1,\lambda_2} \\
&\times D^{0*}_{0,\lambda_1-\lambda_2}(\theta_1,\phi_1) \text{ for } 0^+, \\
A^{2^+}_{NR}(\lambda_0,-\lambda_\gamma,\lambda_1,\lambda_2) &= \sum_{\lambda_J} F^{\psi}_{\lambda_\gamma,\lambda_J} D^{1*}_{\lambda_0,\lambda_J-\lambda_\gamma}(\theta_0,\phi_0) \\
&\times F^{2^+}_{\lambda_1,\lambda_2} D^{2*}_{\lambda_J,\lambda_1-\lambda_2}(\theta_1,\phi_1) \text{ for } 2^+.
\end{aligned}$$

Here, helicity-coupling amplitudes $F^{J^P}_{\lambda_1,\lambda_2}$ are related to covariant amplitudes. For $J^P = 0^-$, helicity amplitudes take the same form as that in Eq. (9).

For the 0^+ case, helicity amplitudes are taken as

$$\begin{aligned}
F^{\psi}_{1} &= F^{\psi}_{-1} = \frac{g_{21} r_1^2}{\sqrt{6}} \frac{B_2(r_1)}{B_2(r_1^0)} + \frac{g_{01}}{\sqrt{3}}, \\
F^{0^+}_{11} &= F^{0^+}_{11} = \frac{g'_{22} r_2^2}{\sqrt{6}} \frac{B_2(r_2)}{B_2(r_2^0)} + \frac{g'_{00}}{\sqrt{3}}, \\
F^{0^+}_{00} &= \sqrt{\frac{2}{3}} r_2^2 g'_{22} \frac{B_2(r_2)}{B_2(r_2^0)} - \frac{g'_{00}}{\sqrt{3}}.
\end{aligned} \tag{10}$$

For the 2^+ case, helicity amplitudes are taken as

$$\begin{aligned}
F^{\psi}_{12} &= F^{\psi}_{-1-2} = \frac{g_{43} r_1^4}{\sqrt{70}} \frac{B_4(r_1)}{B_4(r_1^0)} + \frac{g_{21} r_1^2}{\sqrt{10}} \frac{B_2(r_1)}{B_2(r_1^0)} \\
&- \frac{g_{22} r_1^2}{\sqrt{6}} \frac{B_2(r_1)}{B_2(r_1^0)} + \sqrt{\frac{2}{105}} g_{23} r_1^2 \frac{B_2(r_1)}{B_2(r_1^0)} + \frac{g_{01}}{\sqrt{5}},
\end{aligned} \tag{11}$$

$$\begin{aligned}
F^{\psi}_{11} &= F^{\psi}_{-1-1} = \frac{-2 g_{43} r_1^4}{\sqrt{35}} \frac{B_4(r_1)}{B_4(r_1^0)} - \frac{g_{21} r_1^2}{\sqrt{5}} \frac{B_2(r_1)}{B_2(r_1^0)} \\
&+ \sqrt{\frac{3}{35}} g_{23} r_1^2 \frac{B_2(r_1)}{B_2(r_1^0)} + \frac{g_{01}}{\sqrt{10}},
\end{aligned} \tag{12}$$

$$\begin{aligned}
F^{\psi}_{10} &= F^{\psi}_{-10} = \sqrt{\frac{3}{35}} g_{43} r_1^4 \frac{B_4(r_1)}{B_4(r_1^0)} + \frac{g_{21} r_1^2}{2\sqrt{15}} \frac{B_2(r_1)}{B_2(r_1^0)} \\
&+ \frac{1}{2} g_{22} r_1^2 \frac{B_2(r_1)}{B_2(r_1^0)} + \frac{2 g_{23} r_1^2}{\sqrt{35}} \frac{B_2(r_1)}{B_2(r_1^0)} + \frac{g_{01}}{\sqrt{30}},
\end{aligned} \tag{13}$$

$$\begin{aligned}
F^{2^+}_{11} &= F^{2^+}_{-1-1} = \sqrt{\frac{3}{35}} g'_{42} \frac{B_4(r)}{B_4(r')} r^4 + \frac{g'_{20} r_2^2}{\sqrt{3}} \frac{B_2(r_2)}{B_2(r_2^0)} \\
&- \frac{g'_{22} r_2^2}{\sqrt{21}} \frac{B_2(r_2)}{B_2(r_2^0)} + \frac{g'_{02}}{\sqrt{30}},
\end{aligned} \tag{14}$$

$$\begin{aligned}
F^{2^+}_{10} &= F^{2^+}_{-10} = -\frac{2}{\sqrt{35}} g'_{42} r^4 \frac{B_4(r)}{B_4(r')} - \frac{1}{2} g'_{21} r_2^2 \frac{B_2(r_2)}{B_2(r_2^0)} \\
&- \frac{g'_{22} r_2^2}{2\sqrt{7}} \frac{B_2(r_2)}{B_2(r_2^0)} + \frac{g'_{02}}{\sqrt{10}},
\end{aligned} \tag{15}$$

$$\begin{aligned}
F^{2^+}_{1-1} &= F^{2^+}_{-11} = \frac{g_{42} r^4}{\sqrt{70}} \frac{B_4(r)}{B_4(r')} + \sqrt{\frac{2}{7}} g'_{22} r_2^2 \frac{B_2(r_2)}{B_2(r_2^0)} \\
&+ \frac{g'_{02}}{\sqrt{5}}.
\end{aligned} \tag{16}$$

For these nonresonant decays, the differences of momenta r_l^0 are calculated at the value $m_{\phi\phi} = 2.55$ GeV.

The total amplitude is expressed by:

$$\begin{aligned}
A(\lambda_0,\lambda_\gamma,\lambda_1,\lambda_2) &= A_{\eta_c}(\lambda_0,\lambda_\gamma,\lambda_1,\lambda_2) \\
&+ \sum_{J^P} A^{J^P}_{NR}(\lambda_0,\lambda_\gamma,\lambda_1,\lambda_2),
\end{aligned} \tag{17}$$

where the sum runs over $J^P = 0^-, 0^+$ and 2^+, and the symmetry of identical particle for two ϕ mesons is implied by exchanging their helicities and momentum. The differential cross section is given by

$$\begin{aligned}
d\Gamma &= \left(\frac{3}{8\pi^2}\right) \sum_{\lambda_0,\lambda_\gamma,\lambda_1,\lambda_2} A(\lambda_0,\lambda_\gamma,\lambda_1,\lambda_2) \\
&\times A^*(\lambda_0,\lambda_\gamma,\lambda_1,\lambda_2) d\Phi,
\end{aligned} \tag{18}$$

where $\lambda_0, \lambda_\gamma = \pm 1$, and $\lambda_1, \lambda_2 = \pm 1, 0$, and $d\Phi$ is the element of standard three-body phase space.

B. FIT METHOD

The relative magnitudes and phases for coupling constants are determined by an unbinned maximum likelihood fit. The joint probability density for observing N events in the data sample is

$$\mathcal{L} = \prod_{i=1}^{N} P(x_i), \tag{19}$$

where $P(x_i)$ is a probability to produce event i with a set of four-vector momentum $x_i = (p_\gamma, p_\phi, p_\phi)_i$. The normalized $P(x_i)$ is calculated from the differential cross section

$$P(x_i) = \frac{(d\Gamma/d\Phi)_i}{\sigma_{MC}}, \tag{20}$$

where the normalization factor σ_{MC} is calculated from a MC sample with N_{MC} accepted events, which are generated with a phase space model and then subject to the detector simulation, and are passed through the same event selection criteria as applied to the data analysis. With a MC sample of sufficiently large size, the σ_{MC} is evaluated with

$$\sigma_{MC} = \frac{1}{N_{MC}} \sum_{i=1}^{N_{MC}} \left(\frac{d\Gamma}{d\Phi}\right)_i . \quad (21)$$

For technical reasons, rather than maximizing $\mathcal{L}$, $S = -\ln\mathcal{L}$ is minimized using the package MINUIT. To subtract the background events, the $\ln\mathcal{L}$ function is replaced with

$$\ln\mathcal{L} = \ln\mathcal{L}_{\rm data} - \ln\mathcal{L}_{\rm bg}. \quad (22)$$

After the parameters are determined in the fit, the signal yields of a given resonance can be estimated by scaling its cross section ratio R_i to the number of net events, *i.e.*,

$$N_i = R_i * (N_{\rm obs} - N_{\rm bg}), \text{ with } R_i = \frac{\Gamma_i}{\Gamma_{\rm tot}}, \quad (23)$$

where Γ_i is the cross section for the ith resonance, $\Gamma_{\rm tot}$ is the total cross section, and $N_{\rm obs}$ and $N_{\rm bg}$ are the numbers of observed events and background events, respectively.

The statistical error, δN_i, associated with signal yields N_i is estimated based on the covariance matrix, V, obtained from the fit according to

$$\delta N_i^2 = \sum_{m=1}^{N_{\rm pars}} \sum_{n=1}^{N_{\rm pars}} \left(\frac{\partial N_i}{\partial X_m}\frac{\partial N_i}{\partial X_n}\right)_{\mathbf{X}=\mu} V_{mn}(\mathbf{X}), \quad (24)$$

where $\mathbf{X}$ is a vector containing parameters, and μ contains the fitted values for all parameters. The sum runs over all $N_{\rm pars}$ parameters.

C. RESULTS OF PARAMETERS

The nominal fit includes the decays, $J/\psi \to \gamma\eta_c \to \gamma\phi\phi$ and $J/\psi \to \gamma(\phi\phi)_{J^P} \to \gamma\phi\phi$ with $J^P = 0^-, 0^+, 2^+$. The coupling constants g_{ls} are taken as complex numbers, and they are recombined to give new reduced parameters, which are determined in the fit. The reduced parameters are listed in Table III, and the fitted values are given in Table IV.

TABLE III: Definition of reduced parameters for decays in the nominal fit.

Decays	Reduced parameters
$J/\psi \to \gamma\eta_c \to \gamma\phi\phi$	$N_0 = g_{11}g'_{11}$
$J/\psi \to \gamma(\phi\phi)_{0^-} \to \gamma\phi\phi$	$N_1 = g_{11}g'_{11}$
$J/\psi \to \gamma(\phi\phi)_{2^+} \to \gamma\phi\phi$	$N_2 = g_{43}g'_{22}, \tilde{g}_{21} = g_{21}/g_{43},$
	$\tilde{g}_{22} = g_{22}/g_{43}, \tilde{g}_{23} = g_{23}/g_{43},$
	$\tilde{g}_{20} = g_{20}/g_{43}, \tilde{g}'_{20} = g'_{20}/g'_{22},$
	$\tilde{g}'_{21} = g'_{21}/g'_{22}, \tilde{g}'_{02} = g'_{02}/g'_{22},$
	$\tilde{g}'_{42} = g'_{42}/g'_{22}$
$J/\psi \to \gamma(\phi\phi)_{0^+} \to \gamma\phi\phi$	$N_3 = g_{01}g'_{00}, \tilde{h}_{21} = g_{21}/g_{01},$
	$\tilde{h}'_{22} = g'_{22}/g'_{00}.$

TABLE IV: The values of reduced parameters determined in the nominal fit.

Parameter z	Magnitude $\lvert z\rvert$	Argument $\arg(z)$ $/(2\pi)$
N0	0.11 ± 0.01	0.65 ± 0.05
N1	0.12 ± 0.01	0.13 ± 0.05
N2	0.59 ± 0.27	0.87 ± 0.07
$\tilde{g}_{21}$	0.29±0.12	0.59±0.07
$\tilde{g}_{22}$	0.36±0.14	0.90±0.07
$\tilde{g}_{23}$	0.43± 0.31	0.96±0.11
$\tilde{g}_{20}$	0.07±0.04	0.54±0.10
$\tilde{g}'_{20}$	1.00±0.54	0.61±0.09
$\tilde{g}'_{21}$	0.00±0.51	0.21±0.34
$\tilde{g}'_{02}$	0.66± 0.28	0.50±0.08
$\tilde{g}'_{42}$	0.59±0.26	0.50±0.08
N3	0.01 ± 0.00	0.52 ± 0.07
$\tilde{h}'_{21}$	1.00±0.90	0.99±0.98
$\tilde{h}'_{22}$	2.35±1.25	0.89±0.09

[1] R. Patridge, C. Peck, F. Porter, *et al.*, Phys. Rev. Lett. **45**, 1150(1980);
T. M. Himel, G. H. Trilling, G. S. Abrams, *et al.*, Phys. Rev. Lett. **45**, 1146(1980).

[2] K. A. Olive *et al.* (Particle Data Group), Chin. Phys. C **38**, 090001 (2014).

[3] R. M. Baltrusaitis *et al.* (MARK-III Collaboration), Phys. Rev. Lett. **52**, 2126 (1984).

[4] J. Z. Bai *et al.* (BES Collaboration), Phys. Lett. B **578**, 16 (2004).

[5] M. Ablikim *et al.* (BES Collaboration), Phys. Rev. D **72**, 072005 (2005).

[6] S. J. Brodsky and G. P. Lepage, Phys. Rev. D **24**, 2848 (1981).

[7] V. L. Chernyak and A. R. Zhitnitsky, Nucl. Phys. B**201**, 492 (1982); Nucl. Phys. B**214**, 547 (1983).

[8] Xiao-Hai Liu and Qiang Zhao, Phys. Rev. D **81**, 014017 (2010).

[9] B. Gong, Y. Jia, and J. X. Wang, Phys. Lett. B **670**, 350 (2009);
Y. Jia, Phys. Rev. D **78**, 054003 (2008).

[10] Y. Jia and G. D. Zhao, High Energy Phys. Nucl. Phys. **23**, 765 (1999) (in Chinese).

[11] Peng Sun, Gang Hao, and Cong-Feng Qiao, Phys. Lett. B **702**, 49 (2011).

[12] M. Benayoun, V.L. Chernyak, and I.R. Zhitnitsky, Nucl. Phys. B**348**, 327 (1991);
M. Anselmino, F. Murgia, and F. Caruso, Phys. Rev. D **42**, 3218 (1990).

[13] H. Q. Zhou *et al.*, Phys. Rev. D **71**, 114002 (2005).

[14] Qian Wang, Xiao-Hai Liu, and Qiang Zhao, Phys. Lett. B **711**, 364 (2012).

[15] Z. Q. Liu *et al.* (Belle Collaboration), Phys. Rev. Lett. **108**, 232001 (2012).

[16] M. Ablikim *et al.* (BESIII Collaboration), Chin. Phys. C**41**, 013001 (2017).

[17] M. Ablikim *et al.* (BESIII Collaboration), Nucl. Instrum. Methods Phys. Res., Sect. A **614**, 345 (2010).

[18] J. Z. Bai *et al.* (BES Collaboration), Nucl. Instrum. Methods Phys. Res., Sect. A **458**, 627 (2001); J. Z. Bai *et al.* (BES Collaboration), Nucl. Instrum. Methods Phys. Res., Sect. A **344**, 319 (1994).

[19] D. M. Asner *et al.*, International Journal of Modern Physics **A24** S1, 305-325(2009).

[20] S. Agostinelli *et al.* (GEANT4 Collaboration), Nucl. Instrum. Methods Phys. Res., Sect. A **506**, 250 (2003).

[21] S. Jadach, B. F. L. Ward, and Z. Was, Comput. Phys. Commun. **130**, 260 (2000);
S. Jadach, B. F. L. Ward, and Z. Was, Phys. Rev. D **63**, 113009 (2001).

[22] D. J. Lange, Nucl. Instrum. Methods Phys. Res., Sect. A **462**, 152 (2001);
Ping Rong-Gang, Nucl. Chin. Phys. C **32**, 599 (2008).

[23] J. C. Chen, G. Huang, X. Qi, D. Zhang, and Y. Zhu, Phys. Rev. D **62**, 034003 (2000);
Yang Rui-Ling, Ping Rong-Gang, and Chen Hong, Chin. Phys. Lett. **31**, 061301 (2014).

[24] W. D. Li *et al.*, in $Proceedings of CHEP06, Mumbai, India$, 2006, edited by Sunanda Banerjee (Tata Institute of Fundamental Research, Mumbai, 2006).

[25] S. U. Chung, Phys. Rev. D **57**, 431 (1998);
S. U. Chung, Phys. Rev. D **48**, 1225 (1993).

[26] R. E. Mitchell *et al.* (CLEO Collaboration), Phys. Rev. Lett. **102**, 011801 (2009); R. E. Mitchell *et al.* (CLEO Collaboration),Phys. Rev. Lett. **106**, 159903(E) (2011).

[27] F. James, CERN Program Library Long Writeup D **506** (1998).

[28] M. Ablikim *et al.* (BESIII Collaboration), Phys. Rev. Lett. **108**, 222002 (2012).

[29] M. Ablikim *et al.* (BESIII Collaboration), Phys. Rev. D **83**, 112005 (2011).

[30] D. Bisello *et al.* (DM2 Collaboration), Nucl. Phys. B**350**, 1 (1991).